

Data-Driven Recursive Kinetic Modeling for Fenton Reaction

Tian-Wei Hua, Gui-Xiang Huang*, Chen Qian, Hou-Wei Zeng, Jun Jiang, and Han-Qing Yu*



Cite This: <https://doi.org/10.1021/acs.est.5c06048>



Read Online

ACCESS |

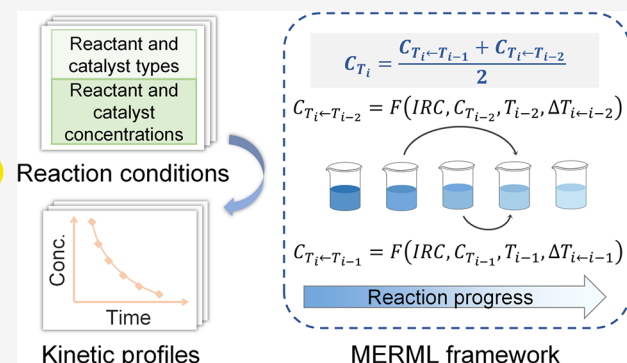
Metrics & More

Article Recommendations

Supporting Information

ABSTRACT: The Fenton reaction is a widely used advanced oxidation process for water purification, valued for its simplicity and effectiveness in degrading refractory organic pollutants. However, accurately modeling its degradation kinetics remains challenging due to the complex reaction mechanism and strong sensitivity to multiple operational variables. Here, we develop a **multiple estimation recursive machine learning (MERML) framework** that is capable of predicting kinetic profiles from initial reaction conditions, including pollutant type, initial pollutant concentration, and Fenton reagent dosages. The MERML, without requiring prior mechanistic knowledge, captures recursive kinetic patterns directly from experimental data by establishing a data-driven mapping from preceding reaction states to future concentrations. This framework demonstrates superior performance in terms of accuracy, few-shot learning capability, robustness, interpretability, and application scope on an experimental data set from Fenton reactions of 12 phenolic compounds. Moreover, MERML enabled data-driven kinetic analysis, including reaction condition optimization, analysis of rate-influencing variables, and identification of representative kinetic patterns. This work provides a novel tool for pollutant degradation modeling, treatment optimization, and kinetic analysis of environmental reaction systems.

KEYWORDS: Fenton reaction, kinetic model, machine learning, recursive relationship, multiestimation strategy



INTRODUCTION

The Fenton reaction is a widely employed advanced oxidation process (AOP) in wastewater treatment, extensively used for the elimination of refractory contaminants.^{1–3} Its widespread adoption stems from its operational simplicity and the ability to generate highly reactive hydroxyl radicals capable of degrading a broad spectrum of contaminants.⁴ Despite its practical success, accurately predicting and effectively controlling degradation behavior under varying conditions remains a significant challenge in Fenton applications. This is because the process is governed by a complex network of reactions that are highly sensitive to factors such as pollutant types and concentrations, reagent dosages, pH, and temperature.^{5,6} The strong interaction among these variables further complicates the prediction of the system performance across diverse treatment scenarios. Therefore, establishing a reliable and broadly applicable understanding of the reaction kinetics is essential not only for elucidating the underlying mechanisms but also for enabling process optimization and dynamic control in real-world applications.^{7–9}

Previous modeling efforts for Fenton kinetics can be broadly categorized into two main approaches. Statistical kinetic models (e.g., pseudononth-order forms) offer broad applicability but often lack accuracy for mechanism-complex systems and struggle when kinetics deviate from simple rate laws.¹⁰ Ordinary differential equations (ODEs)-based kinetic models

can achieve high fidelity for given conditions, but they are typically tailored to specific systems and are difficult to transfer across pollutants or ranges of reaction conditions, and for systems with uncertain or highly complex mechanisms, model construction itself is nontrivial.¹¹ Moreover, both families face difficulty simultaneously accounting for multiple coupled factors, such as pollutant species, initial concentration, reagent dosages, pH, and temperature. These limitations have partly restricted the **practical use of kinetic models**.

To overcome these limitations, a data-driven approach offers a complementary route. Compared with classical models based on explicit equations (e.g., pseudononth-order equations and ODEs), data-driven recursive models provide a more flexible and adaptive means to describe complex nonlinear kinetic patterns,^{12–14} especially when reactions deviate from simple rate laws. Additionally, data-driven recursive models can uncover kinetic relationships directly from data without requiring prior mechanistic assumptions, making them particularly suitable for systems with uncertain or highly

Received: May 6, 2025

Revised: October 29, 2025

Accepted: October 29, 2025

complex mechanisms. Moreover, their ability to incorporate multiple influencing factors makes them highly applicable to Fenton reaction systems,^{15,16} where the kinetic behaviors are influenced by diverse variables, such as pollutant type, Fenton reagent dosage, pH, and temperature.

In this work, we developed a data-driven kinetic modeling framework that is capable of integrating pollutant type, initial pollutant concentration, and Fenton reagent dosages to predict pollutant degradation kinetic profiles. The framework, referred to as Multiple Estimation Recursive Machine Learning (MERML), learns recurrence mappings from preceding reaction states and initial reaction conditions to future pollutant concentrations directly from data and incorporates a multiestimation strategy to enhance prediction performance. We constructed an experimental data set from batch Fenton reactions of various phenolic compounds, which has typical kinetic complexity (Text S1) and whose oxidation intermediates exhibit autocatalytic effects (Figure S4), increasing kinetic complexity.^{17–19} Accordingly, we established and evaluated the MERML on this data set, which demonstrated high predictive accuracy, strong robustness, and good few-shot learning ability. Additionally, we interpreted MERML using post hoc explanation methods and analyzed its internal operational mechanisms. Furthermore, we demonstrated the capability of MERML to perform system-level kinetic analysis, including reaction condition optimization, analysis of parameter effects on reaction rates, and identification of representative kinetic patterns.

MATERIALS AND METHODS

Data Set Construction. The data set was constructed based on the batch Fenton experiments at pH 3.0 ± 0.2 and 25°C , with the specific process described in Text S2. The data set comprises 12 organic reactants (i.e., phenolic pollutants) and 25 concentration groups (i.e., concentrations of pollutants, H_2O_2 and Fe^{2+}) and their corresponding kinetic profiles (sampled at 2, 5, 9, 15, 22, and 30 min), resulting in a total of 300 entries (Figure S5).

MERML Framework. The MERML framework (Figure S6) was developed to predict the complete concentration–time profiles of pollutants in Fenton reactions based on a set of initial reaction conditions (denoted as IRC).

In this framework, the generation of the entire kinetic profiles was fulfilled based on the recursive equation from IRC, previous reaction states (i.e., previous pollutant concentrations and previous reaction time), and time intervals to future pollutant concentrations (eq 1).

$$(\text{IRC}, C_i, T_i, \Delta T_{i-j}) \rightarrow C_j \quad (1)$$

where C_i and T_i are the pollutant concentration and reaction time at the i -th sampling point, respectively. ΔT_{i-j} denotes the time interval between the j -th and i -th sampling point ($j > i$).

A multiestimation strategy was designed to enhance the performance of the framework. In training stage, multiple input-output pairs (as shown in eq 1) could be generated for each target output (i.e., C_j) by selecting different previous reaction states (i.e., C_i and T_i) as inputs. This effectively expanded the training set, acting as a form of data augmentation.²⁰ For the inference stage, multiple predictions could be obtained for each target output by using different previous states as inputs. By averaging these predictions (eq 2),

an ensemble mechanism²¹ was incorporated to further improve the model's accuracy.

$$\hat{C}_j = \frac{\sum_{i=j-k}^{j-1} F(\text{IRC}, \hat{C}_i, T_i, \Delta T_{j-i})}{k} \quad (2)$$

where \hat{C}_i is the final predicted pollutant at the i -th sampling point. k (a user defined hyperparameter) denotes the number of used different previous reaction states to predict pollutant concentrations at target time.

Model Training. Appropriate data preprocessing was conducted to ensure the suitability of the database for constructing the MERML. The initial concentrations of Fe^{2+} and H_2O_2 were converted into the ratios (denoted as [F] and [H], respectively) relative to that of the organic reactant ([OR]). The chemical structures of the phenolic pollutants were encoded as the molecular descriptors based on the 2D topological structure (i.e., Morgan²² fingerprints) and 3D coordinate (i.e., WHIM²³). All of these preprocessed variables and the concentration ratio of Fe^{2+} to H_2O_2 (F/H) were utilized as inputs for the MERML. All of the input variables are listed in Table S1.

The data set was randomly split into training and test sets in an 8:2 ratio using a group-wise procedure: for each reaction, all of its sampling-time data were assigned together to either the training or the test set to prevent potential data leakage.²⁴ The basic components of the MERML were determined through 5-fold validation²⁵ on the training set. We jointly selected the molecular feature representation and the learning algorithm. Among the candidate pairs, the concatenated Morgan and WHIM descriptors with an XGBoost algorithm²⁶ achieved the best cross-validated performance (Figure S7a). To mitigate the potential influence of outliers, the Huber loss function²⁷ was employed for the XGBoost algorithm. Next, the hyperparameters, including the number of previous reaction states used in the inputs, the times of multiple estimation, and the intrinsic hyper-parameters of the XGBoost algorithm were determined. As shown in Figure S7b,c, the optimal number of previous reaction states used in the inputs and times of multiple estimation were determined as 1 and 3, respectively. The intrinsic hyper-parameters were optimized through a grid search, with all optimized hyper-parameters of the MERML displayed in Table S2.

Model Evaluation. The predictive performance of the MERML was evaluated using determination coefficient (eq 3, R^2), mean absolute error (eq 4, MAE), and root mean squared error (eq 5, RMSE) as metric.

$$R^2 = 1 - \frac{\sum_{i=1}^N (c_i - \hat{c}_i)^2}{\sum_{i=1}^N (c_i - \bar{c}_i)^2} \quad (3)$$

$$\text{MAE} = \frac{1}{N} \sum_{i=1}^N |c_i - \hat{c}_i| \quad (4)$$

$$\text{RMSE} = \sqrt{\frac{1}{N} \sum_{i=1}^N (c_i - \hat{c}_i)^2} \quad (5)$$

where N is the number of observations, and c_i and \hat{c}_i represent the measured and predicted concentrations of the i -th sample, respectively.

Model Interpretation. The interpretability of MERML was explored using the SHapley Additive exPlanations (SHAP)

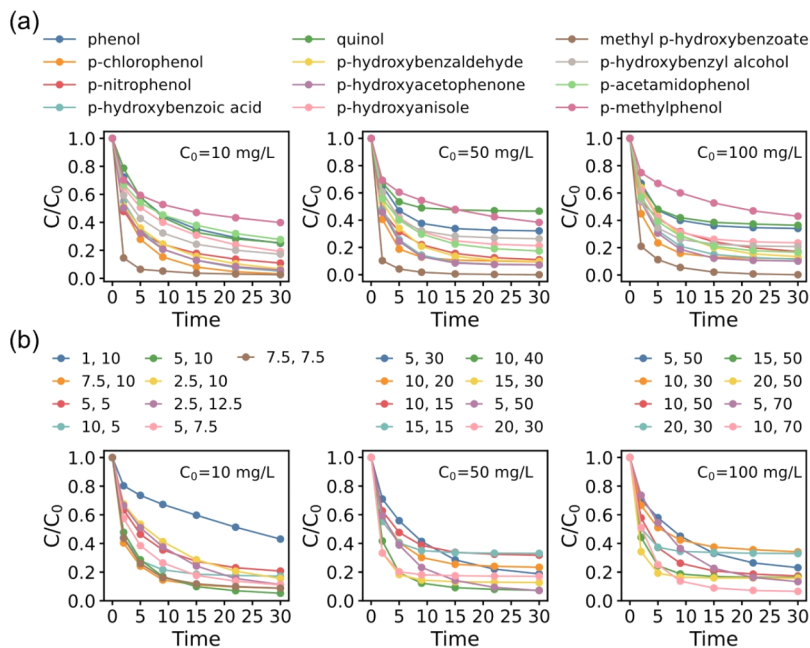


Figure 1. Average degradation profiles across pollutants and reagent concentration combinations. (a) Average degradation profiles for each pollutant, obtained by averaging the concentration–time curves across all concentration combinations of Fe^{2+} and H_2O_2 dosages. (b) Average degradation profiles for each reagent concentration combination, obtained by averaging the concentration–time curves of 12 phenolic pollutants under the same Fe^{2+} and H_2O_2 concentrations. C_0 represents the initial pollutant concentration.

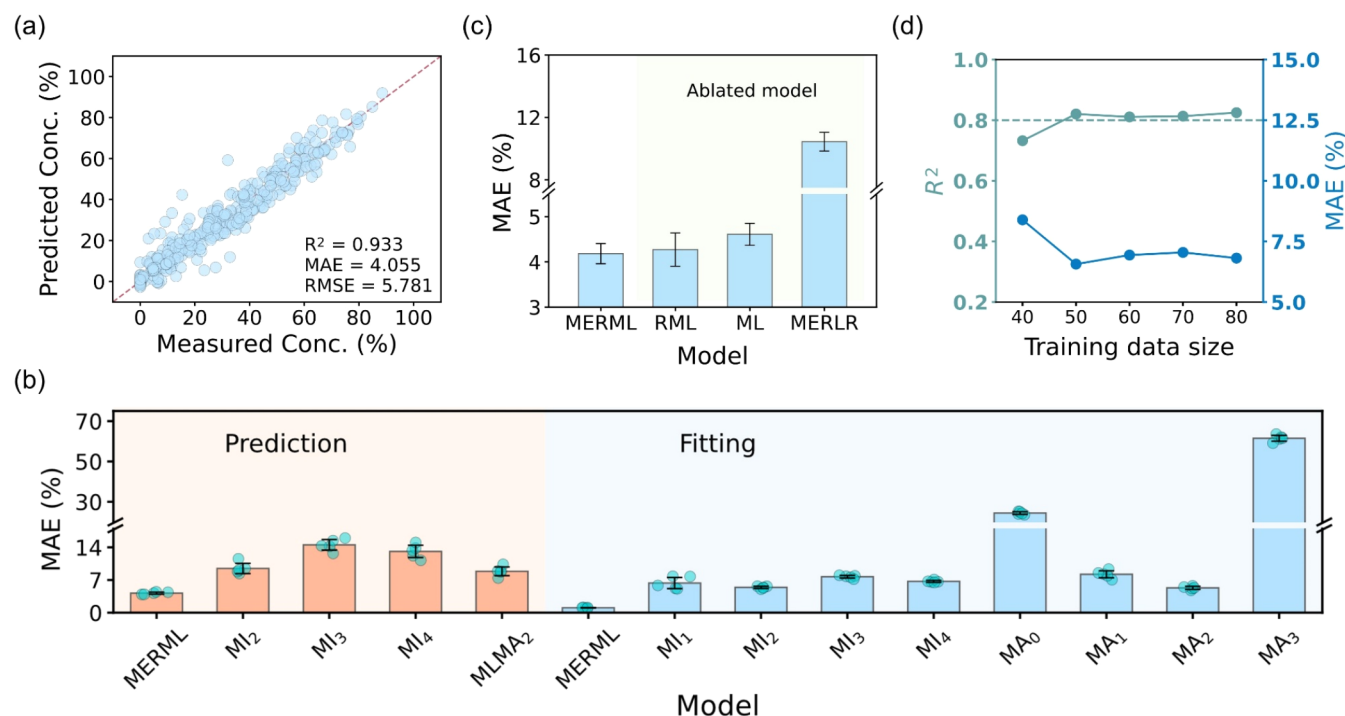


Figure 2. Accuracy of the MERML performance. (a) Regression performance of the MERML on the test set. (b) Predictive and fitting accuracies of the MERML and baseline models. MLMA₂ is a hybrid model that integrates a machine learning algorithm with a pseudo-second-order kinetic equation. Details are described in Text S4.1, S4.2, and S4.3. (c) Predictive accuracy of the MERML and its ablated variants. Details are described in Text S4.4. (d) Regression performances of the MERML trained with training sets of varying sizes on the test set.

algorithm²⁸ and accumulated local effect²⁹ (ALE) algorithm. SHAP is based on cooperative game theory and assigns each input feature a Shapley value, which quantifies its contribution to an individual prediction. ALE plots, in contrast, analyze how the predicted pollutant concentration changes on average as a feature varies across its range while accounting for correlations

between input and output variables. These two methods are complementary: SHAP focuses on local, sample-specific explanations, whereas ALE provides a global understanding of feature effects. Both algorithms were implemented by using their corresponding Python packages.

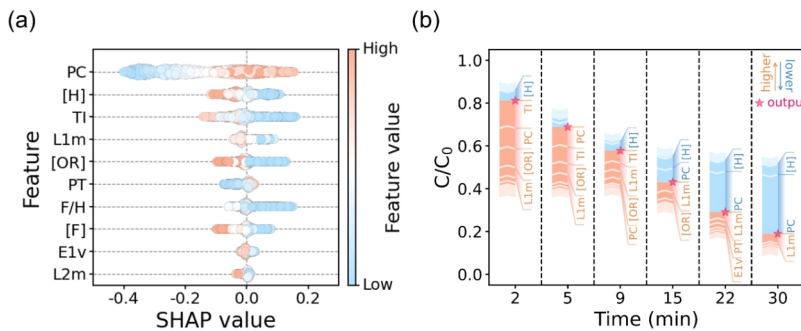


Figure 3. Interpretability of the MERML. (a) Feature contributions of top 10 important features on all samples, ranking from top to down. The abbreviations used to denote the input features are explained in Table S1. (b) Example (its initial reaction conditions: phenol as the organic reactant, the concentrations of phenol, Fe^{2+} , and H_2O_2 are 10, 2.5, and 10 mg L^{-1}) of the adaptive mechanism of the MERML. Orange indicates predictors contributing to higher prediction value of the reactant concentration while blue indicates lower, relative to the base value of 0.45.

RESULTS AND DISCUSSION

Analysis of the Kinetic Data. To support model development and ensure data transparency, we conducted exploratory data analysis of the raw kinetic data. A descriptive analysis (Figure S8) was first conducted by generating summary plots through the averaging of the degradation curves. Specifically, for each pollutant, the profiles under all 25 concentration conditions were averaged to reveal general decay patterns (Figure 1a). In parallel, for each reaction condition, the curves across all 12 pollutants were averaged to examine the influence of reagent dosages (Figure 1b). These plots consistently show a characteristic two-phase behavior: rapid initial degradation followed by a slower secondary stage. Moreover, they confirm that higher Fe^{2+} and H_2O_2 concentrations accelerated degradation, while reagent limitations, particularly H_2O_2 deficiency, led to reduced or incomplete reaction progress.

In addition, a dimensionality-reduction visualization (Text S3.1.3) of all kinetic profiles highlights pronounced heterogeneity and complexity: no single pseudo-order rate law fits all curves, and most profiles deviate substantially from pseudo-order behavior. While, correlation analysis (Text S3.2.2) shows clear linear relationships between pollutant concentrations at different sampling times; notably, the concentration at a given time point is often strongly correlated with concentrations at multiple other time points.

Accuracy of the MERML Framework. The performance of the MERML was systematically evaluated in terms of accuracy, few-shot learning ability,³⁰ robustness, interpretability, and application scope. The predictive accuracy of MERML was first evaluated. As shown in Figure 2a, the MERML demonstrated good predictive performance with predicted values closely matching the experimental data. The results yielded a determination coefficient (R^2) of 0.933, mean absolute error (MAE) of 4.1%, and root mean squared error (RMSE) of 5.8%. According to a previously established threshold,¹⁵ such performance is sufficient for kinetic model-based mechanistic interpretation.

We further compared MERML with a range of classical kinetic models, including macro-kinetic formulations such as pseudozero- (MA_0), first- (MA_1), second- (MA_2), and third-order (MA_3) kinetics, as well as several literature-reported microkinetic models (MI_1 – MI_4).^{31–34} These models were primarily designed for curve fitting and often exhibit limited predictive accuracy when applied to new reaction scenarios due to their reliance on condition-specific rate constants. As a

result, the fitted parameters were typically not transferable to unseen conditions, which limits their generalizability. We first evaluated the fitting errors of classical kinetic models and the MERML by comparing their ability to describe the kinetic behavior observed in the known data set. As shown in Figure 2b, MERML achieved lower fitting errors, highlighting its superior accuracy. Next, the predictive performances on new reaction conditions of the MERML and reference models were evaluated. The MERML exhibited substantially lower prediction errors (Figure 2b), demonstrating its superior predictive accuracy. This is likely because the reference model's kinetic parameters were dependent on reaction conditions (Figure S12d–f). As a result, the parameters fitted to the training data might not remain valid when extrapolated to new scenarios in the test set.

To better understand the source of MERML's predictive accuracy, we conducted ablation experiments by systematically removing key components of the model architecture. Specifically, we created three ablated versions of MERML by individually removing the multiple estimation strategy, the recursive modeling scheme, or replacing the machine learning component with a linear regression model, and the corresponding models were named RML, ML, and MERLR, respectively. As shown in Figure 2c, all of these ablated models exhibited noticeably higher prediction errors compared to the full MERML architecture, highlighting the importance of each component in achieving high predictive accuracy.

We also evaluated the MERML's few-shot learning capability,³⁰ where conventional machine learning models often face limitations. The few-shot learning ability was evaluated based on the accuracies of the MERML trained on a small-sized training data set. The model presented acceptable accuracy ($R^2 > 0.8$) when the training set size reached 50 (Figure 2d), demonstrating its ability to address the challenges of building large experimental data sets. Additionally, the MERML presented better accuracy than RML and ML ones on the small training set, with the latter two presenting similar accuracy (Figure S16). This indicates that the good few-shot learning ability was attributed to the usage of the multiple estimation strategy that might have an effect of enhancing training data set.

The robustness of MERML was explored under two typical scenarios encountered in kinetic studies: the presence of experimental noise and missing concentration–time points. In both cases, MERML consistently outperformed the ablated models, maintaining high prediction accuracy (Figure S17).

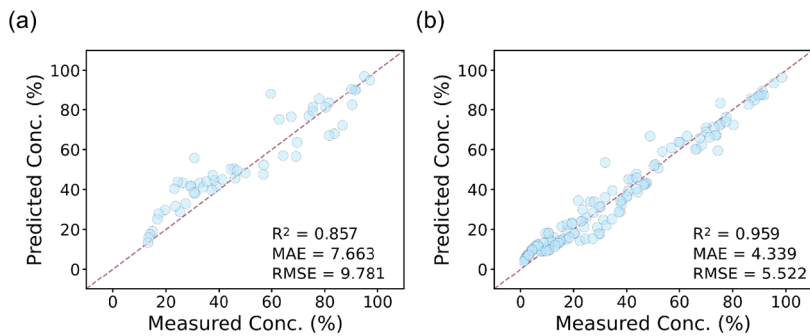


Figure 4. General applicability of the MERML. (a) Prediction performance of the MERML on the Fenton reactions of nonphenolic pollutants (i.e., DOHF and MP). (b) Prediction performance of the MERML model for the photocatalytic degradation of bisphenol A.

These results highlight the model's strong error tolerance and its ability to handle incomplete or noisy data sets, which can be attributed to the integration of recursive modeling and the multiple estimation strategy. This robustness is especially valuable in wastewater treatment, where data noise and loss are common, enhancing MERML's suitability for real-world applications.

Interpretability of the MERML Framework. To understand how the MERML generates its predictions, we conducted feature attribution analysis using SHAP and ALE algorithms. The results (Figure 3a) show that the features related to recursive relation construction, including the pollutant concentration at the previous pollutant concentrations (PC), the time interval between previous and current time points (TI), and previous reaction time (PT), ranked higher in importance than the initial reaction conditions, such as Fe^{2+} and H_2O_2 dosages. This result suggests that MERML primarily relied on recent reaction history to generate predictions, while initial conditions played a supporting role in refining the prediction. This reliance on dynamic reaction history, rather than fixed condition-specific parameters, might partially explain MERML's ability to generalize across diverse reaction scenarios.

Moreover, analysis of feature contributions as the reaction progressed revealed a dynamic adjustment process, which we define as an adaptive mechanism. This behavior arises from the incorporation of recursive relationships in MERML, which implicitly introduces information on previous reaction states, including PC, PT, and average reaction rate (PC/PT), into the input features. Thus, the MERML becomes aware of the prior reaction history and automatically adjusts the influence of initial conditions on the reaction rate (Figure 3b), enabling it to adapt to both varying initial conditions and ongoing reaction evolution. This adaptive mechanism ensures that the MERML can robustly and accurately predict kinetic profiles across diverse and complex reaction scenarios.

Application Scope of the MERML Framework. In addition, we explored the application scope of MERML. Generally, the application scope of data-driven models is related to the composition of the training data. Thus, for the MERML trained with the current data set, we defined its applicability to Fenton reactions based on the types and concentrations of organic reactants included in the training data set (Table S8). Nevertheless, extrapolation experiments demonstrated that MERML retained reasonable predictive accuracy even for reagent concentrations and phenolic pollutants not included in the training set, indicating a certain

degree of generalization beyond the original data set (Texts S5.1 and S5.2).

Moreover, MERML exhibited great potential for broader applications, as neither the machine learning component nor the recursive framework relied on predefined chemical mechanisms. We found that MERML generalizes well to other pollutant types and to extended reaction conditions (e.g., pH and temperature) within the Fenton system. We evaluated two representative nonphenolic pollutants, including Drimaren Orange HF 2GL³⁵ (DOHF, a reactive azo dye) and methyl parathion³⁶ (MP, an organophosphorus pesticide), under initial conditions specified by temperature, pH, pollutant concentration, Fe^{2+} concentration, and H_2O_2 concentration. The results (Figure 4a) show accurate predictions across these compounds and condition combinations, demonstrating MERML's applicability to chemically diverse substrates and coupled operating factors. Additionally, to explore its transferability to systems beyond Fenton chemistry, we applied MERML to a photocatalytic oxidation reaction governed by quasi-second-order kinetics (Text S6).³⁷ The MERML retrained with this new data set also performed well (Figure 4b). After retraining with the corresponding data set, the model again achieved satisfactory prediction accuracy (Figures S19 and S20), supporting its applicability to other kinetic regimes.

These results underscore the flexibility and extensibility of the MERML framework. By modification of the input feature set to reflect relevant reaction conditions, the model can, in principle, be adapted to a wide variety of chemical systems, including those involving different pollutant classes, oxidants, catalysts, or environmental conditions. As long as sufficient time-resolved experimental data are available, MERML provides a unified approach for kinetic modeling across diverse degradation pathways.

Kinetic Analysis Based on the MERML Framework. The capabilities of the MERML framework in kinetic analysis, in terms of reaction condition optimization, analyzing the impacts of reaction conditions on reaction rates, and identifying representative kinetic patterns, were showcased.

For reaction condition optimization, the model trained on 300 entries was used to rapidly evaluate the other 324 reaction conditions in the application scope that were not tested experimentally. From the total 624 conditions, the optimal concentrations of Fenton reagents (i.e., Fe^{2+} and H_2O_2) could be identified for any given organic reactant type, concentration, and reaction time in the data set. For instance, for 50 mg L⁻¹ quinol, the optimal concentrations of Fe^{2+} and H_2O_2 were 20 and 50 mg L⁻¹ at 2 min and 5 and 40 mg L⁻¹ at 30 min,

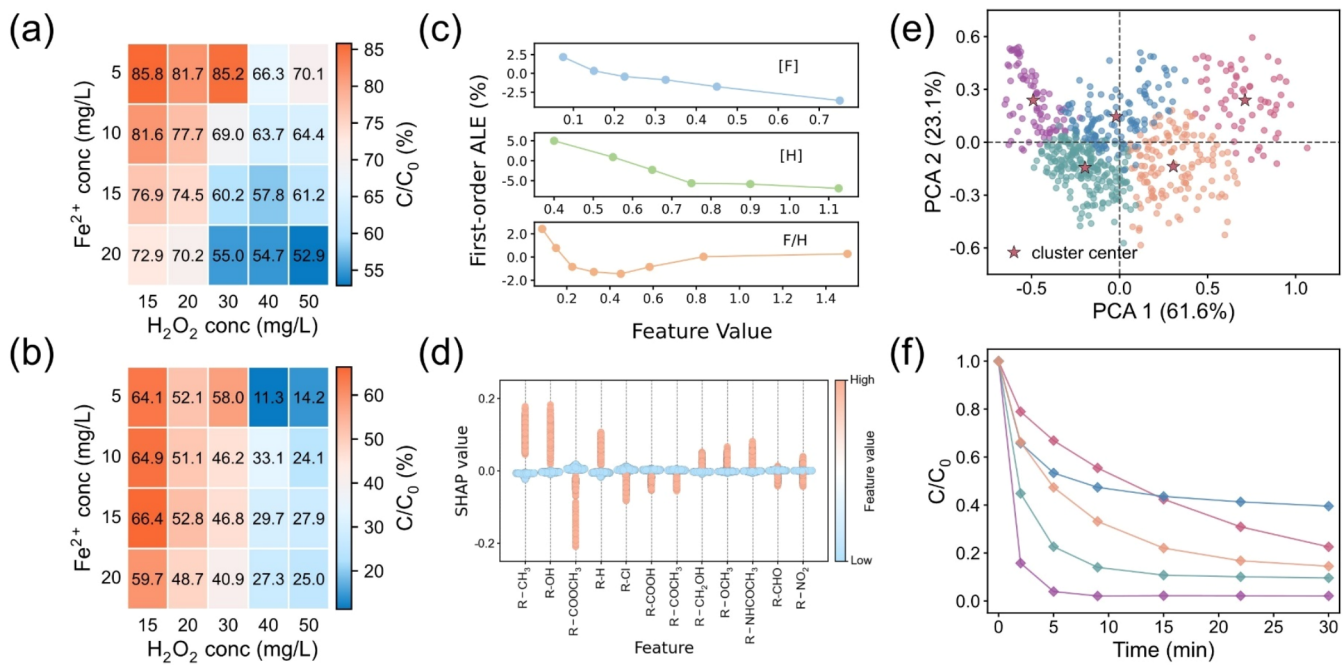


Figure 5. Reaction condition optimization and kinetic analysis based on MERML. (a, b) Predicted remaining pollutant concentrations at 2 and 30 min, respectively, for Fenton reactions of 50 mg L⁻¹ quinol. (c) Effect of the Fe²⁺/H₂O₂ mass concentration ratio on reaction rate. (d) Effect of pollutant molecular structure on reaction rate. (e) K-means clustering result of the kinetic profiles. (f) Representative kinetic profile of each cluster in panel (e).

Table 1. Statistical Result of the Reaction Conditions for the Representative Kinetic Profiles^a

kinetic profile	average concentration		number of pollutant											
	[F]	[H]	A	B	C	D	E	F	G	H	I	J	K	L
blue	0.349	0.529	38	18	21	10	13	15	0	0	6	0	0	2
green	0.388	0.721	1	13	16	17	14	21	27	29	22	29	32	3
purple	0.367	0.706	0	0	0	1	3	1	2	6	7	7	9	43
orange	0.261	0.695	10	14	10	17	12	13	14	13	9	12	9	4
pink	0.133	0.875	3	7	5	7	10	2	9	4	8	4	2	0

^a[H]: the ratio between the concentration of H₂O₂ and initial organic reactant concentration; [F]: the ratio between the concentration of Fe²⁺ and initial organic reactant concentration; The letters from A to L represent *p*-methylphenol, phenol, quinol, *p*-hydroxyanisole, *p*-acetamidophenol, *p*-hydroxybenzyl alcohol, *p*-hydroxybenzaldehyde, *p*-hydroxybenzoic acid, *p*-nitrophenol, *p*-hydroxyacetophenone, *p*-chlorophenol, and methyl *p*-hydroxybenzoate, respectively.

respectively (Figure 5a,b). Notably, the optimal conditions varied significantly over time, highlighting the necessity of the MERML's capability to optimize conditions at any given moment.

Furthermore, the impacts of reaction conditions on reaction rates were also analyzed in terms of reagent concentrations and pollutant structures based on model interpretation. For the former, we analyzed the combined influence of Fe²⁺ and H₂O₂ dosages by assessing the impact of their concentration ratio, to demonstrate the model's capacity to resolve more complex interactive effects between reagents. ALE-based analysis reveals that increasing the Fe²⁺/H₂O₂ mass concentration ratio initially enhances the reaction rate, followed by a decline beyond the optimal ratio of 1:2 (Figure 5c). For the analysis of pollutant structures, we simplified the input representation by replacing hybrid molecular descriptors with one-hot descriptor (Table S15) or Morgan fingerprints (Table S16). SHAP-based analysis reveals that electron-withdrawing groups (e.g., carbonyl group and chlorine atom) at the para position of the hydroxyl group increase the reaction rate of phenolic compounds, while electron-donating groups (e.g., methyl and

methoxy) tend to reduce the rate (Figures 5d and S21 and Table S17). These findings demonstrate that MERML can support data-driven analysis of how multiple reaction conditions and structural features jointly influence the reaction kinetics.

Moreover, MERML was also shown to be effective in identifying representative kinetic patterns. Specifically, the model enables the rapid generation of kinetic profiles under diverse reaction conditions, which can be further statistically analyzed to reveal kinetic patterns. These profiles can be clustered (using K-means algorithms³⁸) by shape, defined through differential vectors of kinetic profiles, with each shape corresponding to a distinct kinetic pattern that may reflect underlying mechanistic differences. As illustrated in Figure 5e, 624 kinetic profiles of the Fenton reactions were obtained and then classified into five groups (Figure 5f). The curves colored pink likely indicate catalyst deactivation due to the insufficient Fe²⁺ concentration (Table 1) disrupting the Fe²⁺/Fe³⁺ cycle.³⁹ The purple curves suggest the fast and complete consumption of organic reactants at the early stage of the Fenton reactions. The curves in blue and green suggest the early termination of

the Fenton reactions due to the deficiency of H₂O₂. In contrast, the curves in orange represent the Fenton reactions that follow pseudo-second-order kinetics (Figure S22), without the special kinetic behaviors mentioned above caused by the insufficiency of Fe²⁺, H₂O₂, or pollutant. These findings demonstrate that the MERML allows systematic classification of reactions that may follow different kinetic patterns and reflect distinct underlying mechanisms.

In summary, in this work, we demonstrated the potential of using recursive relationships to construct a high-performance kinetic model of Fenton reactions through correlation analysis and subsequently proposed a recursive machine learning framework configured with a multiple estimation strategy. The MERML was trained and evaluated using an experimental data set of Fenton reactions. The evaluation results show high accuracy ($R^2 = 0.933$), strong robustness, notable few-shot learning ability, clear interpretability, and broad application scope of the model. Additionally, the strong ability of the model to promote kinetic analysis was also showcased. It could aid in optimizing reaction conditions for any given reaction time, resolving the influence of complex reaction conditions, and identifying typical reaction mechanisms. In the future work, incorporating time-resolved concentrations of peroxide and iron species to strengthen the recursive relationships, along with expanding the diversity of reaction conditions represented in the training data set, is expected to further enhance the predictive performance and applicability of the MERML. Additionally, considering that some methods have been established for predicting the reaction mechanisms based on kinetic profiles,^{15,40,41} integration of the MERML with those methods can be adopted in the future to expedite the overall workflow of chemical kinetic research. Given these capabilities, MERML is expected to contribute meaningfully to environmental applications, particularly in kinetic modeling and optimization of advanced oxidation processes.

ASSOCIATED CONTENT

Data Availability Statement

All data and codes are included in the article and publicly available at <https://github.com/TWH-USC/MERML>.

Supporting Information

The Supporting Information is available free of charge at <https://pubs.acs.org/doi/10.1021/acs.est.5c06048>.

Details of Fenton reactions; complexity of the kinetics of Fenton reaction; description of reference kinetic models; application domain of the MERML for Fenton reaction (PDF)

AUTHOR INFORMATION

Corresponding Authors

Gui-Xiang Huang – State Key Laboratory of Advanced Environmental Technology, Department of Environmental Science and Engineering, University of Science and Technology of China, Hefei 230026, China;  orcid.org/0000-0003-1223-0164; Email: gxhuang@ustc.edu.cn

Han-Qing Yu – State Key Laboratory of Advanced Environmental Technology, Department of Environmental Science and Engineering, University of Science and Technology of China, Hefei 230026, China;  orcid.org/0000-0001-5247-6244; Email: hqyu@ustc.edu.cn

Authors

Tian-Wei Hua – State Key Laboratory of Advanced Environmental Technology, Department of Environmental Science and Engineering, University of Science and Technology of China, Hefei 230026, China;  orcid.org/0009-0000-3728-2767

Chen Qian – State Key Laboratory of Advanced Environmental Technology, Department of Environmental Science and Engineering, University of Science and Technology of China, Hefei 230026, China

Hou-Wei Zeng – State Key Laboratory of Advanced Environmental Technology, Department of Environmental Science and Engineering, University of Science and Technology of China, Hefei 230026, China

Jun Jiang – Hefei National Research Center for Physical Sciences at the Microscale, School of Chemistry and Materials Science, University of Science and Technology of China, Hefei 230026, China;  orcid.org/0000-0002-6116-5605

Complete contact information is available at:
<https://pubs.acs.org/10.1021/acs.est.5c06048>

Notes

The authors declare no competing financial interest.

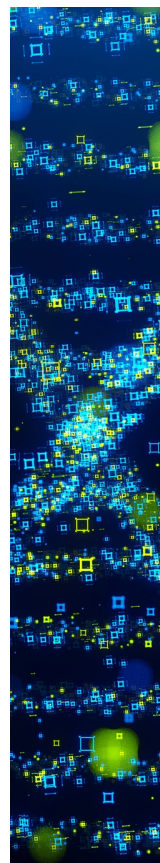
ACKNOWLEDGMENTS

This work was supported by the National Natural Science Foundation of China (52192684, 22376191, 52027815 and 52293443), the Youth Innovation Fund of USTC (WK2400000005), and the Students Innovation and Entrepreneurship Foundation of USTC (SC5290005062).

REFERENCES

- (1) Pacheco-Álvarez, M.; Picos Benítez, R.; Rodríguez-Narváez, O. M.; Brillas, E.; Peralta-Hernández, J. M. A critical review on paracetamol removal from different aqueous matrices by Fenton and Fenton-based processes, and their combined methods. *Chemosphere* **2022**, 303, No. 134883.
- (2) Wang, J.; Zhuan, R. Degradation of antibiotics by advanced oxidation processes: An overview. *Sci. Total Environ.* **2020**, 701, No. 135023.
- (3) Chen, Q.; Lü, F.; Zhang, H.; He, P. Where should Fenton go for the degradation of refractory organic contaminants in wastewater. *Water Res.* **2023**, 229, No. 119479.
- (4) Ribeiro, J. P.; Nunes, M. I. Recent trends and developments in Fenton processes for industrial wastewater treatment – A critical review. *Environ. Res.* **2021**, 197, No. 110957.
- (5) Babuponnusami, A.; Muthukumar, K. A review on Fenton and improvements to the Fenton process for wastewater treatment. *J. Environ. Chem. Eng.* **2014**, 2 (1), 557–572.
- (6) Zhang, M. H.; Dong, H.; Zhao, L.; Wang, D. X.; Meng, D. A review on Fenton process for organic wastewater treatment based on optimization perspective. *Sci. Total Environ.* **2019**, 670, 110–121.
- (7) Duesterberg, C. K.; Waite, T. D. Process optimization of Fenton oxidation using kinetic modeling. *Environ. Sci. Technol.* **2006**, 40 (13), 4189–4195.
- (8) Doumic, L. I.; Haure, P. M.; Cassanello, M. C.; Ayude, M. A. Mineralization and efficiency in the homogeneous Fenton Orange G oxidation. *Appl. Catal., B* **2013**, 142–143, 214–221.
- (9) Du, Y.; Zhou, M.; Lei, L. Kinetic model of 4-CP degradation by Fenton/O₂ system. *Water Res.* **2007**, 41 (5), 1121–1133.
- (10) Motagamwala, A. H.; Dumesic, J. A. Microkinetic Modeling: A Tool for Rational Catalyst Design. *Chem. Rev.* **2021**, 121 (2), 1049–1076.
- (11) Wang, K.; Han, L.; Mustakis, J.; Li, B.; Magano, J.; Damon, D. B.; Dion, A.; Maloney, M. T.; Post, R.; Li, R. Kinetic and Data-Driven

- Reaction Analysis for Pharmaceutical Process Development. *Ind. Eng. Chem. Res.* **2020**, *59* (6), 2409–2421.
- (12) Sani, O. G.; Pesaran, B.; Shanche, M. M. Dissociative and prioritized modeling of behaviorally relevant neural dynamics using recurrent neural networks. *Nat. Neurosci.* **2024**, *27* (10), 2033–2045.
- (13) Vlachas, P. R.; Pathak, J.; Hunt, B. R.; Sapsis, T. P.; Girvan, M.; Ott, E.; Koumoutsakos, P. Backpropagation algorithms and Reservoir Computing in Recurrent Neural Networks for the forecasting of complex spatiotemporal dynamics. *Neural Netw.* **2020**, *126*, 191–217.
- (14) Uriarri, G.; Mindlin, G. B. Dynamical time series embeddings in recurrent neural networks. *Chaos, Solitons Fractals* **2022**, *154*, No. 111612.
- (15) Burés, J.; Larrosa, I. Organic reaction mechanism classification using machine learning. *Nature* **2023**, *613* (7945), 689–695.
- (16) Murakami, Y.; Shono, A. Reaction engineering with recurrent neural network: Kinetic study of Dushman reaction. *Chem. Eng. J. Adv.* **2022**, *9*, No. 100219.
- (17) Li, Y.; Cheng, H. Autocatalytic effect of in situ formed (hydro) quinone intermediates in Fenton and photo-Fenton degradation of non-phenolic aromatic pollutants and chemical kinetic modeling. *Chem. Eng. J.* **2022**, *449*, No. 137812.
- (18) Xiao, J.; Wang, C.; Liu, H. Fenton-like degradation of dimethyl phthalate enhanced by quinone species. *J. Hazard. Mater.* **2020**, *382*, No. 121007.
- (19) Chen, C.; Wang, Y.; Huang, Y.; Hua, J.; Qu, W.; Xia, D.; He, C.; Sharma, V. K.; Shu, D. Overlooked self-catalytic mechanism in phenolic moiety-mediated Fenton-like system: Formation of Fe(III) hydroperoxide complex and co-treatment of refractory pollutants. *Appl. Catal., B* **2023**, *321*, No. 122062.
- (20) Li, B.; Hou, Y.; Che, W. Data augmentation approaches in natural language processing: A survey. *AI Open* **2022**, *3*, 71–90.
- (21) Sagi, O.; Rokach, L. Ensemble learning: A survey. *Wiley Interdiscip. Rev. Data Min. Knowl. Discovery* **2018**, *8* (4), No. e1249.
- (22) Rogers, D.; Hahn, M. Extended-Connectivity Fingerprints. *J. Chem. Inf. Model.* **2010**, *50* (5), 742–754.
- (23) Todeschini, R.; Consonni, V. Descriptors from Molecular Geometry. In *Handbook of Chemoinformatics*; Wiley, 2003; pp 1004–1033.
- (24) Zhang, K.; Zhong, S.; Zhang, H. Predicting Aqueous Adsorption of Organic Compounds onto Biochars, Carbon Nanotubes, Granular Activated Carbons, and Resins with Machine Learning. *Environ. Sci. Technol.* **2020**, *54* (11), 7008–7018.
- (25) Arlot, S.; Celisse, A. A Survey of Cross Validation Procedures for Model Selection. *Stat. Surv.* **2010**, *4*, 40–79.
- (26) Chen, T.; Guestrin, C. In *XGBoost: A Scalable Tree Boosting System*, Proceedings of the 22nd ACM SIGKDD International Conference on Knowledge Discovery and Data Mining, San Francisco, CA, 2016; pp 785–794.
- (27) Huber, P. J. Robust Estimation of a Location Parameter. *Ann. Math. Stat.* **1964**, *35*, 492–518.
- (28) Štrumbelj, E.; Kononenko, I. Explaining prediction models and individual predictions with feature contributions. *Knowl. Inf. Syst.* **2014**, *41* (3), 647–665.
- (29) Apley, D. W.; Zhu, J. Visualizing the effects of predictor variables in black box supervised learning models. *J. R. Stat. Soc. Ser. B* **2020**, *82* (4), 1059–1086.
- (30) Alayrac, J.-B.; Donahue, J.; Luc, P.; Miech, A.; Barr, I.; Hasson, Y.; Lenc, K.; Mensch, A.; Millican, K.; Reynolds, M. Flamingo: a visual language model for few-shot learning, 2022. <https://doi.org/10.48550/arXiv.2204.14198>.
- (31) Wu, Y.; Zhou, S.; Qin, F.; Zheng, K.; Ye, X. Modeling the oxidation kinetics of Fenton's process on the degradation of humic acid. *J. Hazard. Mater.* **2010**, *179* (1), 533–539.
- (32) Sun, J.-H.; Sun, S.-P.; Fan, M.-H.; Guo, H.-Q.; Qiao, L.-P.; Sun, R.-X. A kinetic study on the degradation of p-nitroaniline by Fenton oxidation process. *J. Hazard. Mater.* **2007**, *148* (1–2), 172–177.
- (33) Beltran De Heredia, J.; Torregrosa, J.; Dominguez, J. R.; Peres, J. A. Kinetic model for phenolic compound oxidation by Fenton's reagent. *Chemosphere* **2001**, *45* (1), 85–90.
- (34) Giménez, B. N.; Conte, L. O.; Audino, F.; Schenone, A. V.; Graells, M.; Alfano, O. M.; Pérez-Moya, M. Kinetic model of photo-Fenton degradation of paracetamol in an annular reactor: main reaction intermediates and cytotoxicity studies. *Catal. Today* **2023**, *413–415*, No. 113958.
- (35) Değermenci, N.; Değermenci, G. D.; Ulu, H. B. Decolorization of reactive azo dye from aqueous solutions with Fenton oxidation process: effect of system parameters and kinetic study. *Desalin. Water Treat.* **2019**, *169*, 363–371.
- (36) Saini, R.; Kumar Mondal, M.; Kumar, P. Fenton oxidation of pesticide methyl parathion in aqueous solution: kinetic study of the degradation. *Environ. Prog. Sustainable Energy* **2017**, *36* (2), 420–427.
- (37) Yang, C.; Wang, P.; Li, J.; Wang, Q.; Xu, P.; You, S.; Zheng, Q.; Zhang, G. Photocatalytic PVDF ultrafiltration membrane blended with visible-light responsive Fe(III)-TiO₂ catalyst: Degradation kinetics, catalytic performance and reusability. *Chem. Eng. J.* **2021**, *417*, No. 129340.
- (38) Ahmed, M.; Seraj, R.; Islam, S. M. S. The k-means algorithm: A comprehensive survey and performance evaluation. *Electronics* **2020**, *9* (8), 1295.
- (39) Liu, Z.; Pan, S.; Xu, F.; Wang, Z.; Zhao, C.; Xu, X.; Gao, B.; Li, Q. Revealing the fundamental role of MoO₂ in promoting efficient and stable activation of persulfate by iron carbon based catalysts: Efficient Fe²⁺/Fe³⁺ cycling to generate reactive species. *Water Res.* **2022**, *225*, No. 119142.
- (40) Burés, J. Variable Time Normalization Analysis: General Graphical Elucidation of Reaction Orders from Concentration Profiles. *Angew. Chem., Int. Ed.* **2016**, *55* (52), 16084–16087.
- (41) Blackmond, D. G. Reaction progress kinetic analysis: a powerful methodology for mechanistic studies of complex catalytic reactions. *Angew. Chem., Int. Ed.* **2005**, *44* (28), 4302–4320.



CAS BIOFINDER DISCOVERY PLATFORM™

STOP DIGGING THROUGH DATA — START MAKING DISCOVERIES

CAS BioFinder helps you find the right biological insights in seconds

Start your search

